PCCP

ARTICLE TYPE

Cite this: DOI: 00.0000/xxxxxxxxxx

Supplementary information for "Towards detection of molecular parity violation via chiral co-sensing: the $^{1}H/^{31}P$ model system"

Erik Van Dyke*[a,b], James Eills[c], Kirill Sheberstov[d], John Blanchard[e], Manfred Wagner[f], Andrés Emilio Wedenig[g], Konstantin Gaul*[a,b,g], Robert Berger[g], Rudolf Pietschnig[h], Denis Kargin[h], Danila A. Barskiy*[a,b], and Dmitry Budker[a,b,i]

[a] *Institute for Physics, Johannes Gutenberg University Mainz, 55128 Mainz, Germany.*
[b] *Helmholtz Institute Mainz, 55128 Mainz, Germany; GSI Helmholtz Center for Heavy Ion Research, Darmstadt, Germany.*
[c] *Institute of Biological Information Processing (IBI-7), Forschungszentrum Jülich, Jülich 52425, Germany*
[d] *Laboratoire des biomolécules, LBM, Département de chimie, École normale supérieure, PSL University, Sorbonne Université, CNRS, 75005 Paris, France.*
[e] *Quantum Technology Center, University of Maryland, College Park, Maryland, MD, 20742 USA*
[f] *Max Planck Institute for Polymer Research, 55128 Mainz, Germany.*
[g] *Institute for Chemistry, Philipps University Marburg, 35032 Marburg, Germany.*
[h] *Institute for Chemistry, University of Kassel, 34132 Kassel, Germany.*
[i] *Department of Physics, University of California at Berkeley, Berkeley CA 94720, USA.*
* Corresponding author.

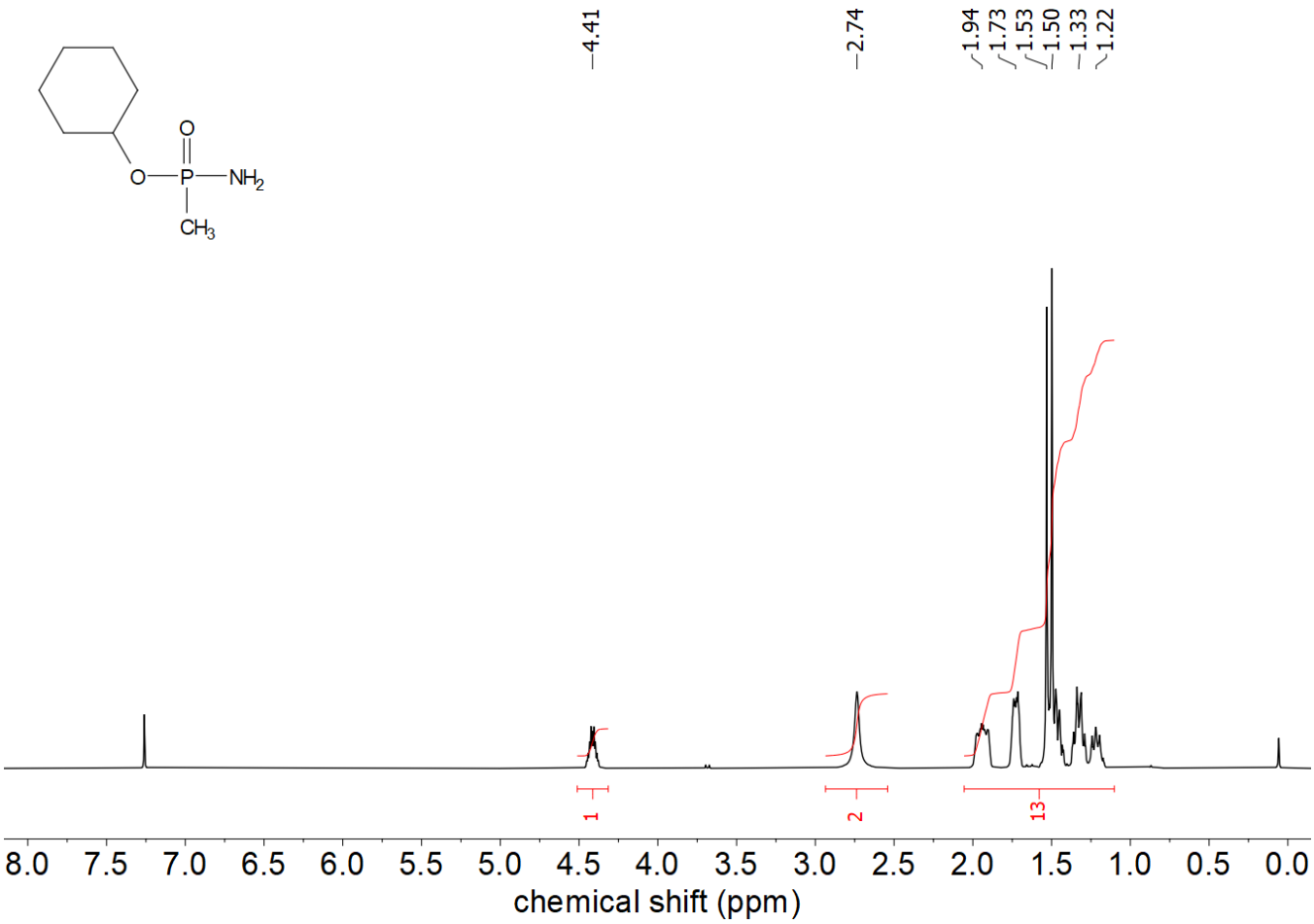

Fig. 1 ^{1}H NMR spectrum (400 MHz, $CDCl_3$) of Cyclohexyl *P*-methylphosphonamidate. The methyl protons used to extract diastereomeric splitting are observed at 1.50 ppm and 1.53 ppm, split by coupling to phosphorus by a *J*-coupling of 16.8 Hz. The residual ^{1}H signal from the chloroform-d solvent at 7.28 ppm is used to reference the spectra.

1 NMR characterization of chiral phosphonamidate

All experiments, if not stated otherwise, were carried out under exclusion of moisture and air under an inert argon atmosphere. Starting materials were purified and stored under argon. Methylphosphonic dichloride was prepared according to literature procedures. Starting from trimethylphosphite and catalytic amounts of methyl iodide, dimethyl methylphosphonate was prepared in an Arbuzov reaction. Thereafter reaction of dimethyl methylphosphonate with thionylchlorid yielded methylphosphonic dichloride. Butyllithium (2.5M in hexanes) was purchased from Merck and used as received. Diethylether was dried over sodium potassium alloy and distilled prior to use. Cyclohexanol was purchased from Merck, dried over sodium and distilled prior to use. Diethylamine was purchased from abcr, dried over CaH and distilled prior to use. For substance preparation and characterisation, NMR spectra were measured with Varian 500VNMRS and Varian MR-400 spectrometers at 298 K. Chemical shifts were referenced to residual protic impurities in the solvent (^{1}H) or the deuterio solvent itself (^{13}C) and reported relative to external $SiMe_4$ (^{1}H, ^{13}C or 85% aqueous H_3PO_4 for ^{31}P).

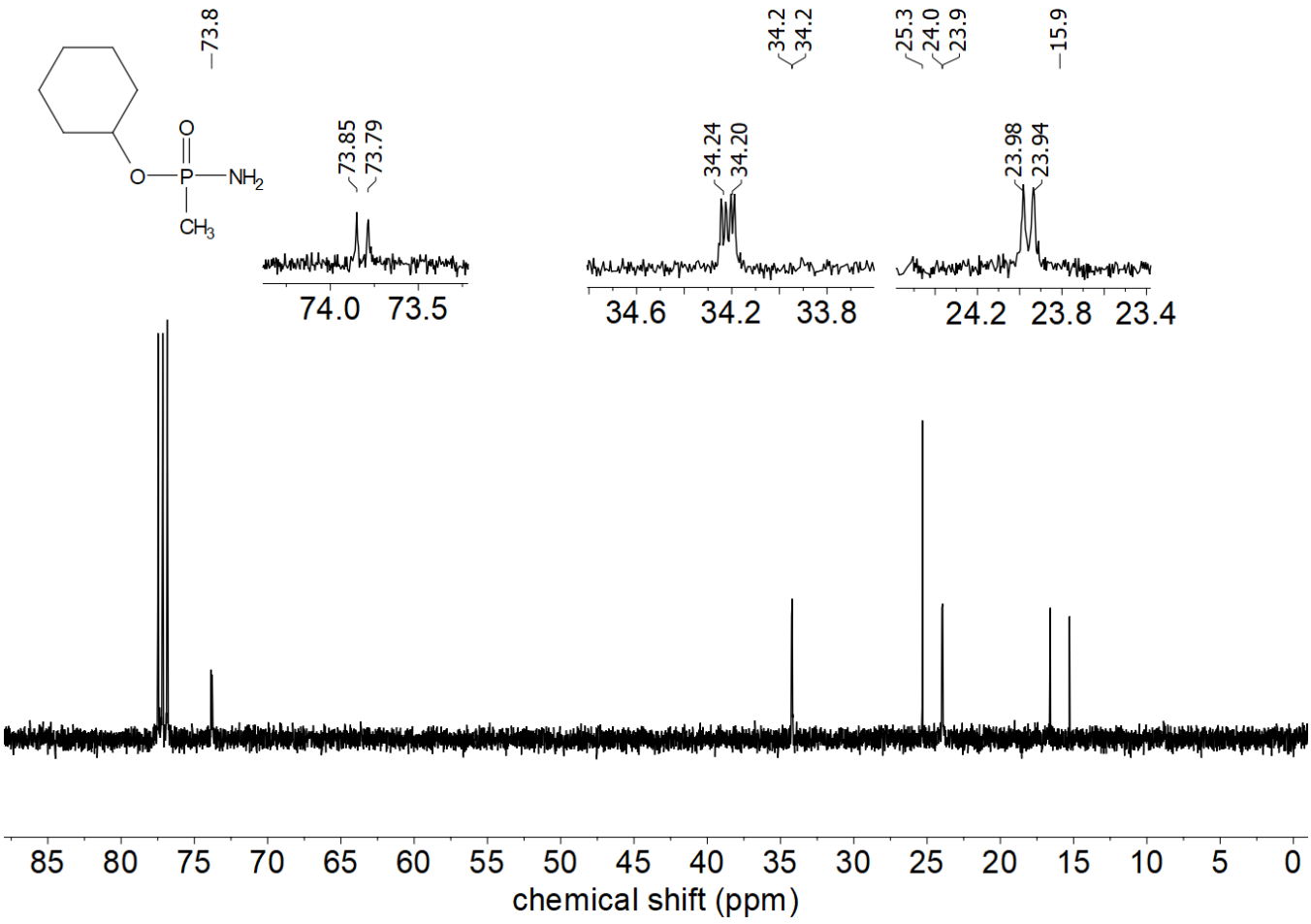

Fig. 2 ^{13}C NMR spectrum (101 MHz, $CDCl_3$) of Cyclohexyl *P*-methylphosphonamidate with selected detail enlargement.

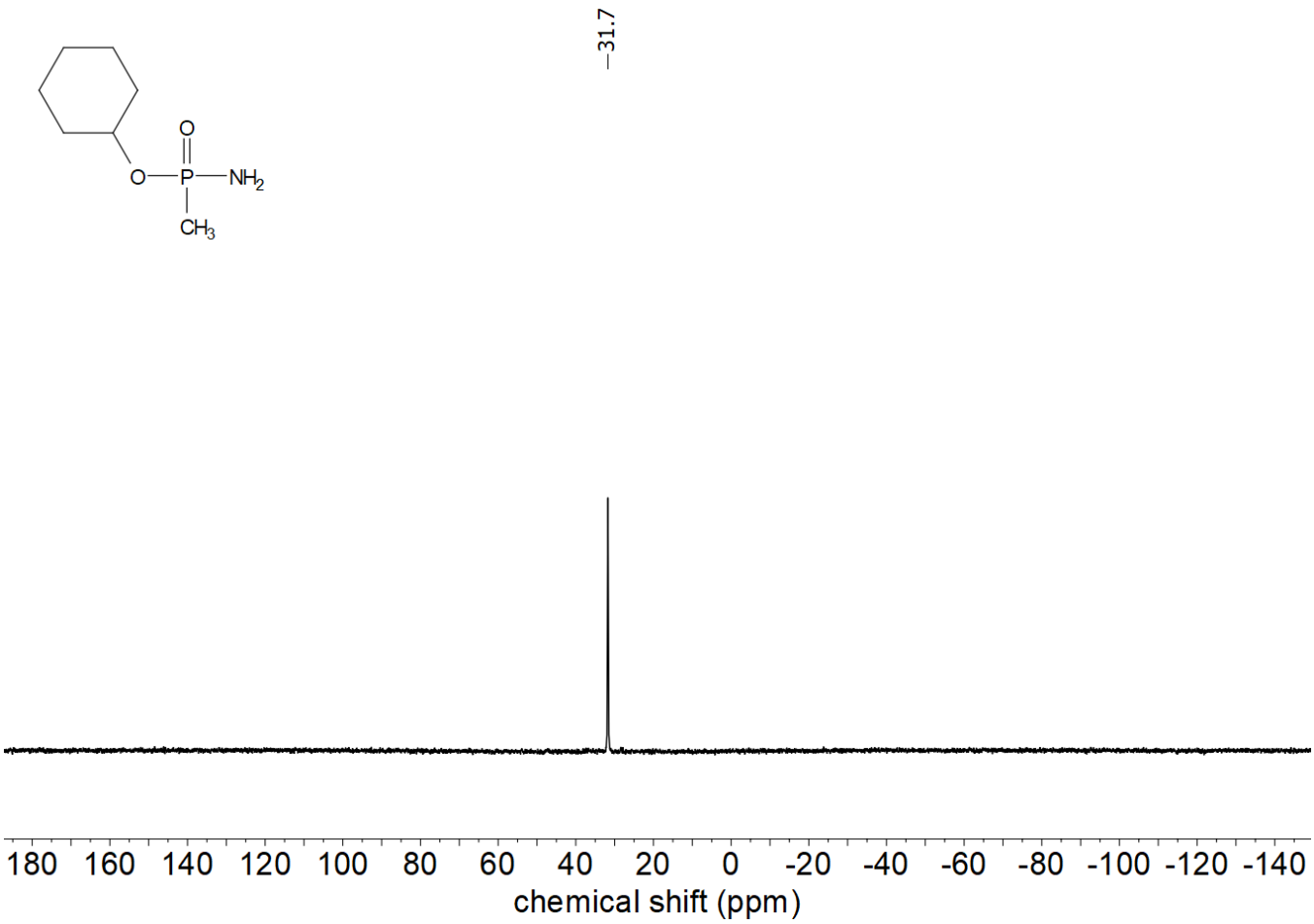

Fig. 3 ^{31}P NMR spectrum (202 MHz, $CDCl_3$) of Cyclohexyl *P*-methylphosphonamidate.

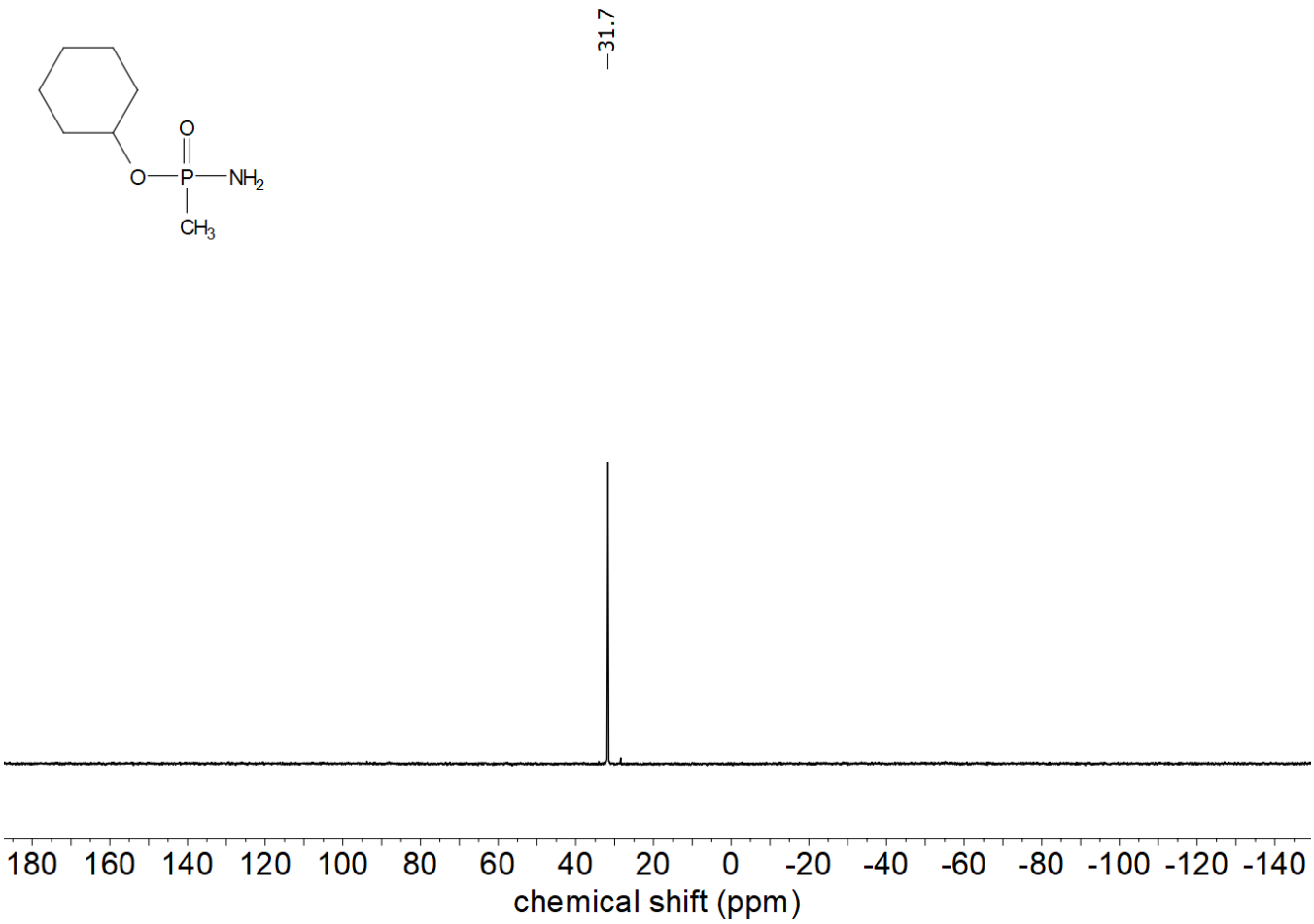

Fig. 4 $^{31}P\{^{1}H\}$ NMR spectrum (202 MHz, $CDCl_3$) of Cyclohexyl *P*-methylphosphonamidate.

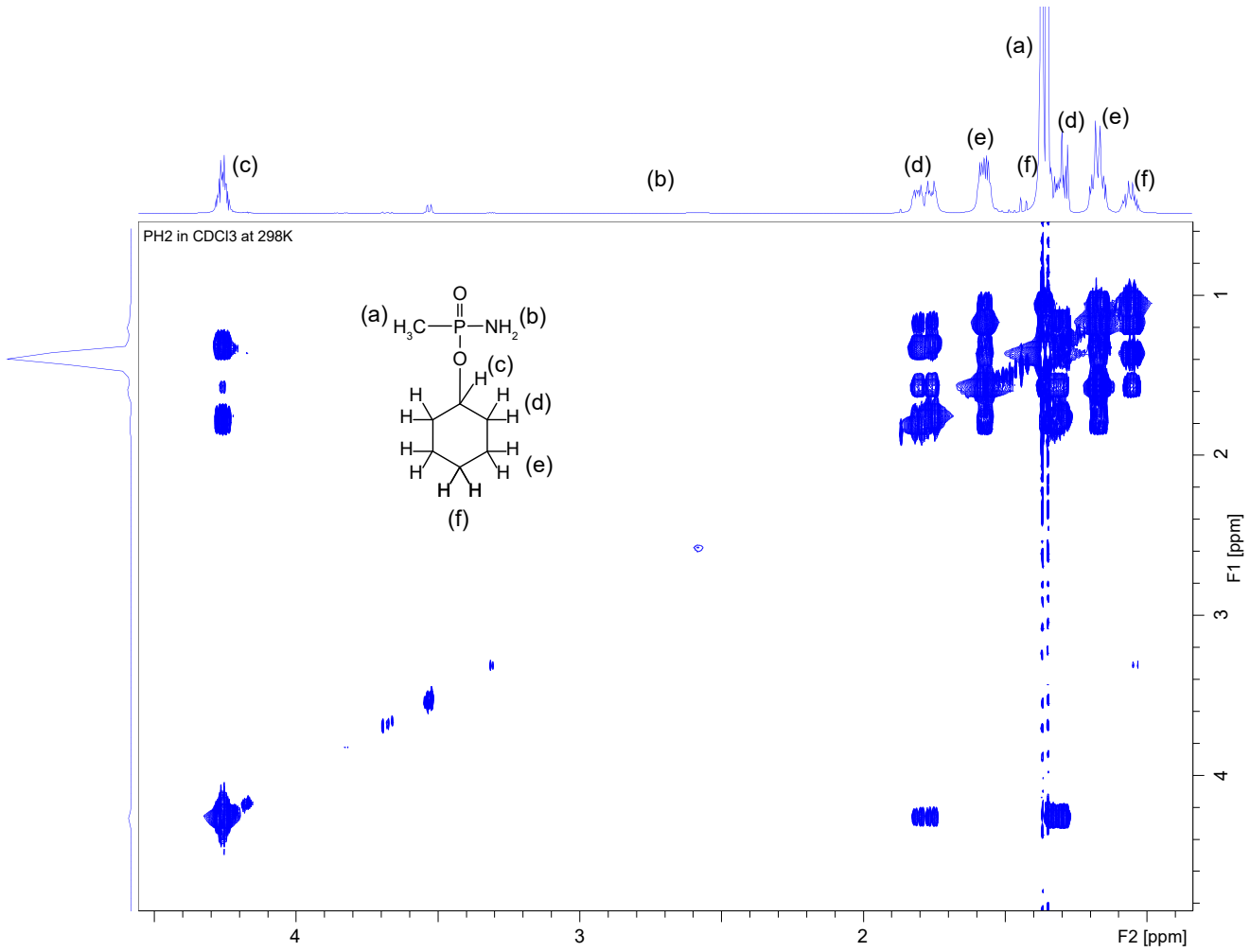

Fig. 5 ^{1}H COSY NMR spectrum (850 MHz, $CDCl_3$, 298 K) of Cyclohexyl *P*-methylphosphonamidate.

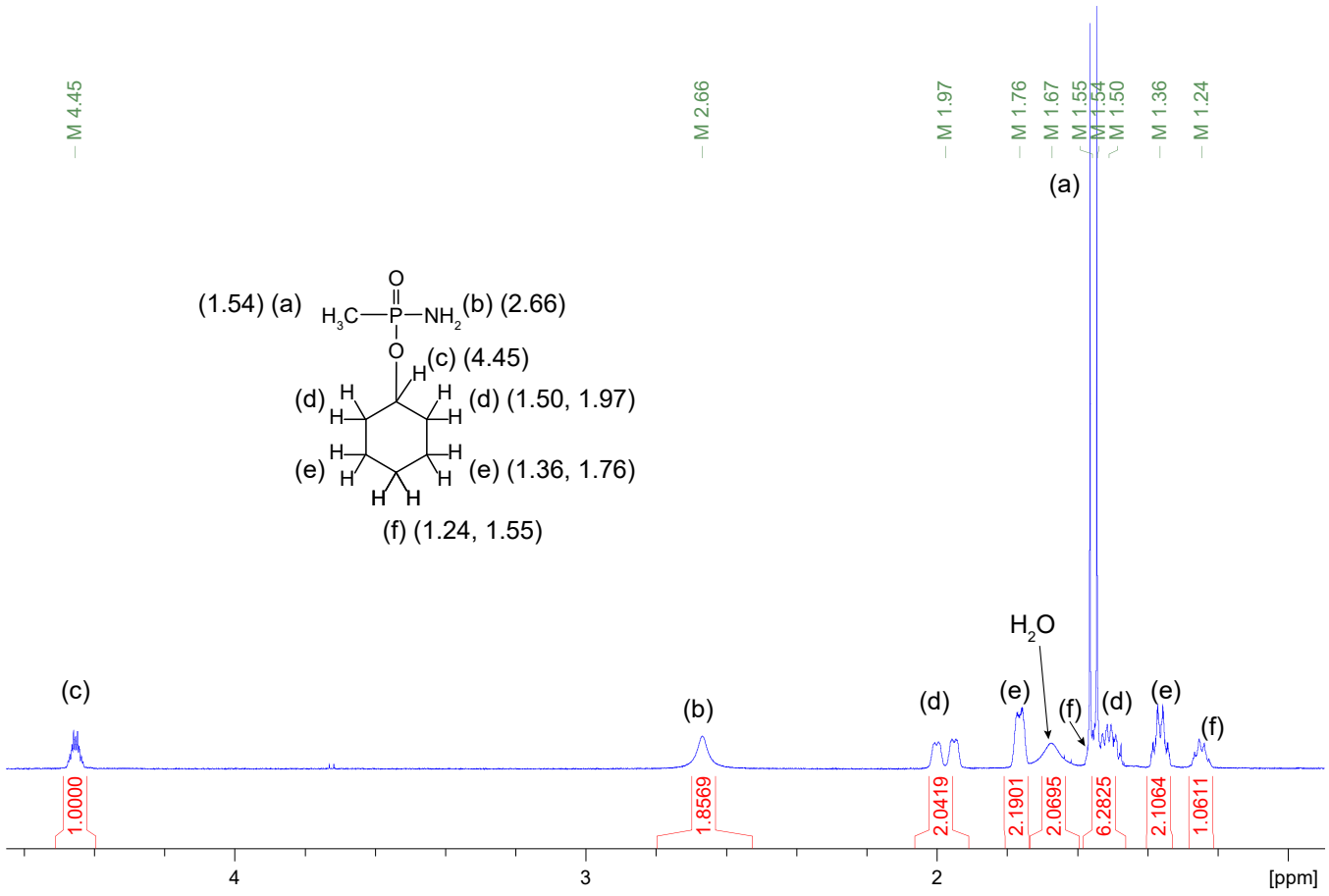

Fig. 6 ^{1}H NMR spectrum (850 MHz, $CDCl_3$, 298 K) of Cyclohexyl *P*-methylphosphonamidate. For ease of interpretation, only peak centers are indicated and splitting due to *J*-coupling is ignored.

2 Examination of diastereomeric splitting of P in the presence of chiral solvating agent

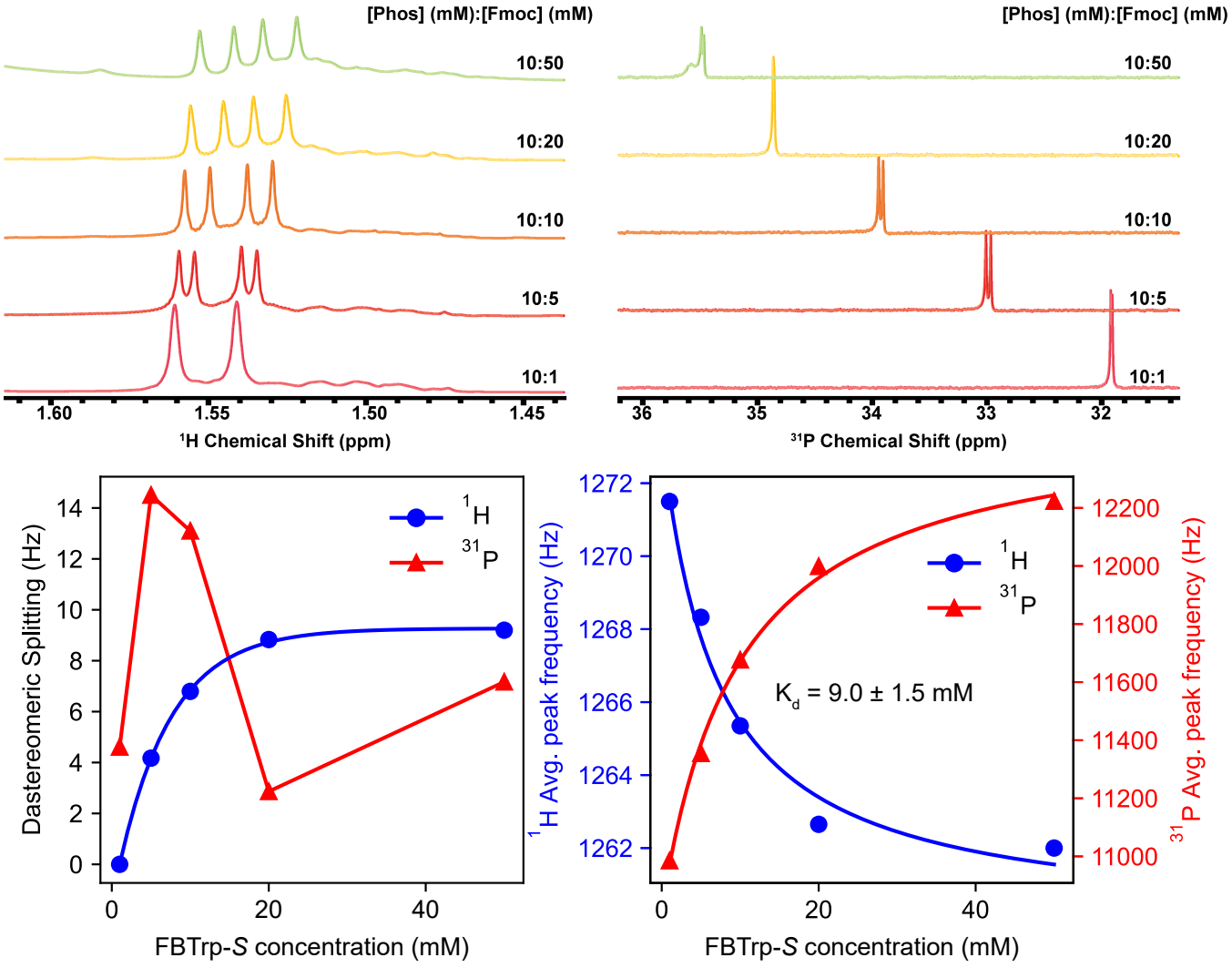

Fig. 7 Increasing the ratio of FBTrp:P with 10 mM P in chloroform-d. ^{1}H spectra (left) shown are the sum of 32 scans and ^{31}P spectra (right) are the sum of 64 scans collected with proton decoupling. While ^{1}H diastereomeric splitting (Δ_d) increases asymptotically to a maximum at $\Delta_d = 9.5$ Hz as the ratio of FBTrp-S:P is increased, $\Delta_d{}^{31}$P increases a point before collapsing at higher FBTrp-S:P. The ratio of 1:1 was chosen for the titration experiments in this study to maximize the total Δ_d with the hopes of maximizing the total precision of the comagnetometry measurement. However since this ratio is outside of the linear regime in both ^{1}H and ^{31}P, changes in concentration of P or FBTrp are likely to cause shifts in Δ_d that are not compensated by the comagnetometry approach. In future experiments, a ratio where changes in splitting of both nuclei are linear should be chosen. Binding affinity is determined from the shift in peak frequency of both ^{1}H and ^{31}P spectra using the model

$$\delta_{\text{obs}} = \delta_{\text{free}} + (\delta_{\text{free}} - \delta_{\text{bound}})\frac{K_d}{[L] + K_d},$$

where K_d is the dissociation constant, δ_{obs} is the observed chemical shift, δ_{free} is the chemical shift of the free species, δ_{bound} is the chemical shift of the bound species, and $[L]$ is the concentration of FBTrp-S. The reported K_d is the weighted average of values given by fits of ^{1}H (7.0 ± 2.9 mM) and ^{31}P (10.0 ± 1.8 mM) average peak frequencies.

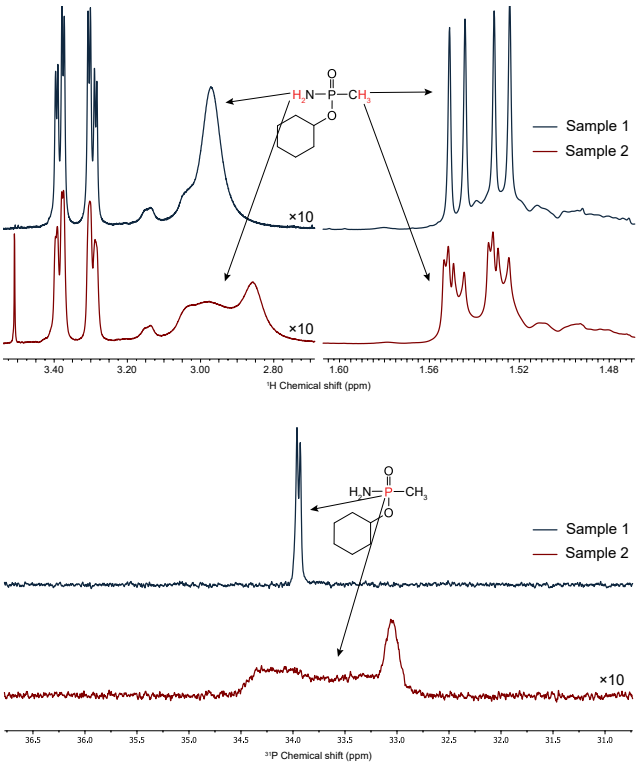

Fig. 8 Example of sample degradation observed in a sample with 10 mM P and FBTrp with an enantiomeric ratio of 6% FBTrp-S in chloroform-d. The top ^{1}H and ^{31}P spectra are of a sample which did not display sample degradation over a 24 hour storage period at 4 °C. The bottom ^{1}H and ^{31}P spectra are of different sample with the same concentrations of P and FBTrp in the same chloroform-d solvent but from a different bottle, with clear signs of the formation of additional species due to unspecified chemical reactions.

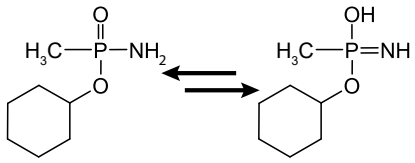

Fig. 9 Imine-amine tautomerization may occur in the probe molecule, creating the highly reactive imine. This may explain the sample degradation observed in some samples which was seemingly dependent on the storage and age of the solvent chloroform-d used to prepare the samples.

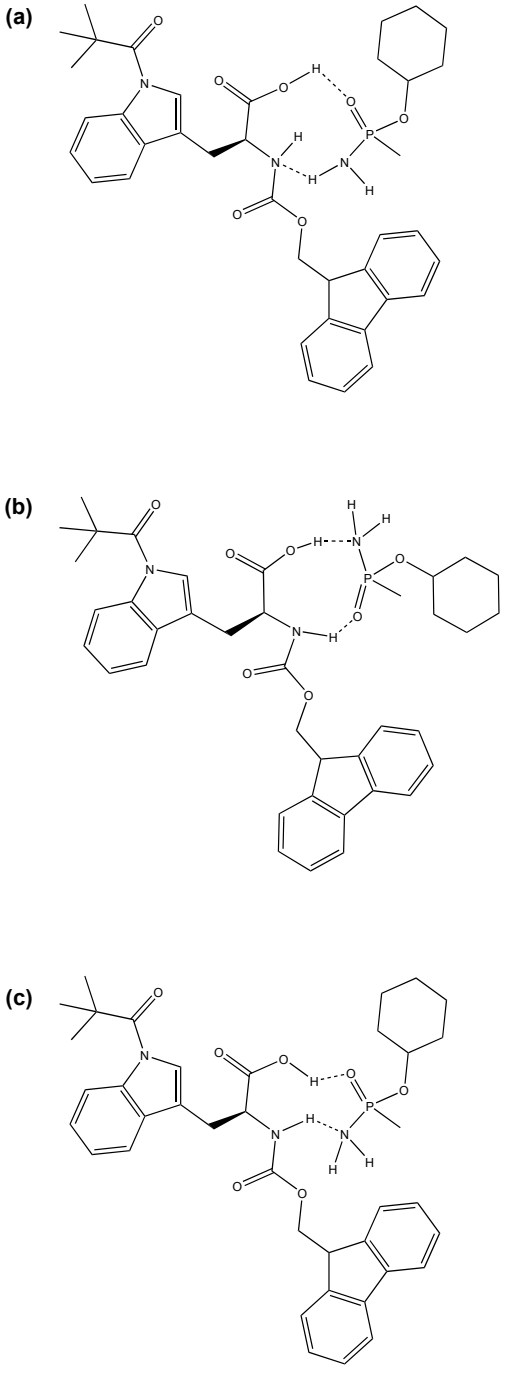

Fig. 10 Binding interactions between the chiral phosphonamidate P and substituted tryptophan FBTrp could be mediated by two groups on each molecule, namely the phosphoryl oxygen and amino moieties of P and the carboxylic acid and amino moieties of FBTrp. This work did not include characterization of this binding interaction, however the structures shown here depict likely binding interactions that may occur.

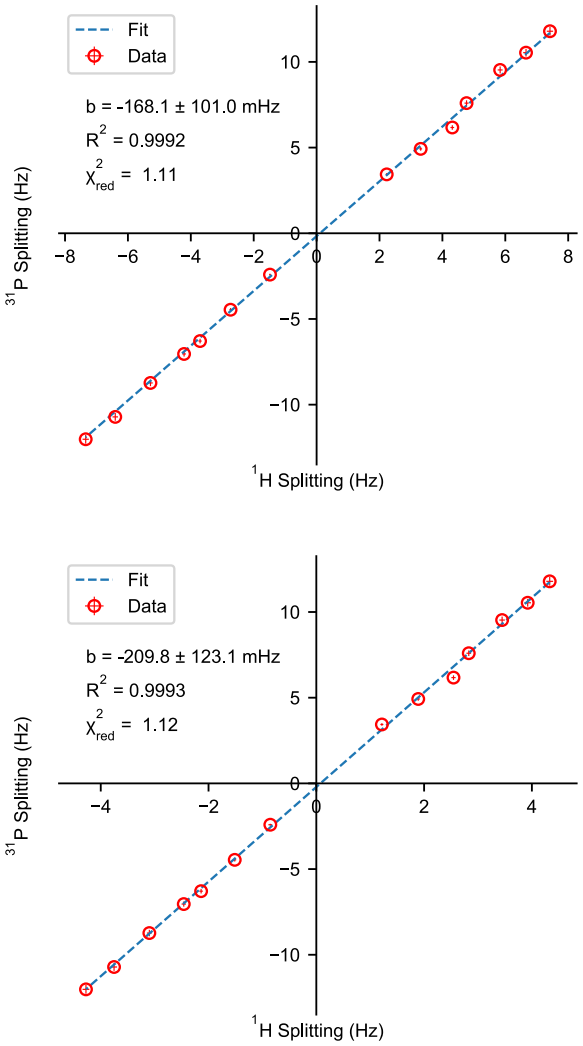

Fig. 11 Comagnetometry plot showing diastereomeric splitting in spectra of P complexed with FBTrp as a function of ^{1}H diastereomeric splitting two ^{1}H multiplets. Both ^{31}P and ^{1}H spectra were collected using a 90° pulse, with ^{1}H decoupling on ^{31}P spectra. Reduced chi squared (χ^2_{red}) values of 1.12 and 1.11 indicate the error values used to compute the fit are a good estimation of the actual error, assuming a linear model.

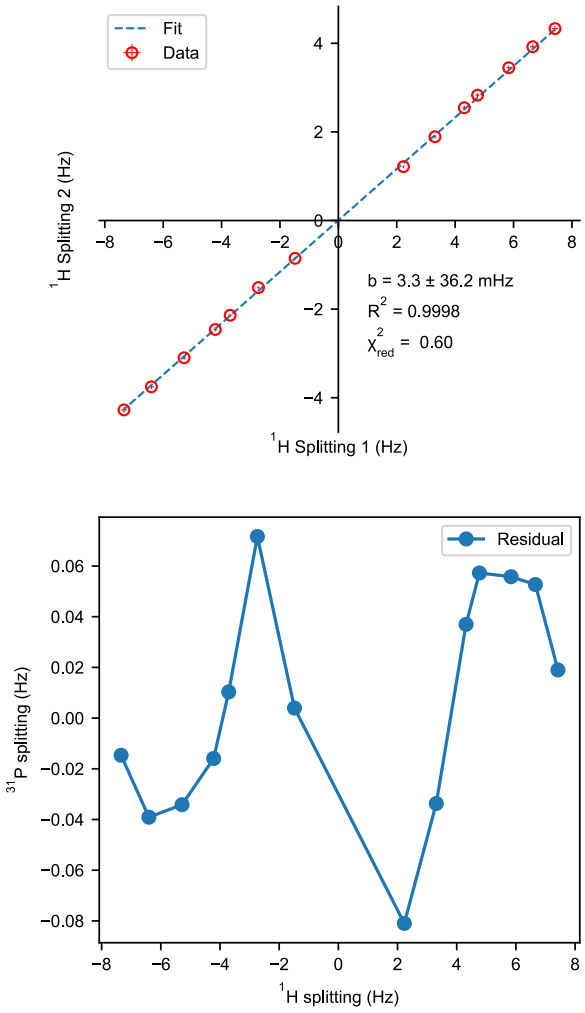

Fig. 12 Comagnetometry plot showing correlation between diastereomeric splitting of two ^{1}H multiplets originating from P. Both horizontal and vertical axis ^{1}H Δ_d values are extracted from spectra of the same samples and show a high degree of correlation. The plot below shows the difference between the fitted line and the measured values.

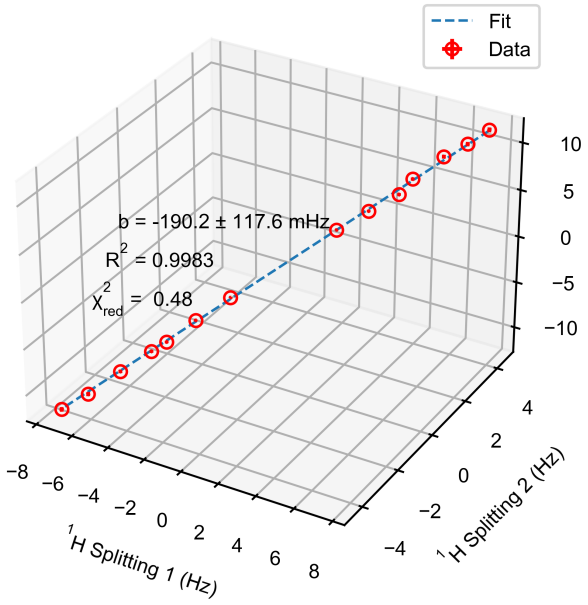

Fig. 13 Plot of ^{31}P splitting as a function of two ^{1}H multiplets originating from P which display diastereomeric splitting. Fitting was accomplished by minimizing $\chi^2 = \sum_i (\frac{y_{obs} - y_{x_i}}{T.E.})^2$ with $T.E. = \sqrt{(a\sigma_x)^2 + (b\sigma_y)^2 + \sigma_c^2 + 2a\rho_{xz}\sigma_x\sigma_y + 2b\rho_{yz}\sigma_y\sigma_z + 2ab\rho_{xy}\sigma_x\sigma_y}$ for the function $z = ax + by + c$

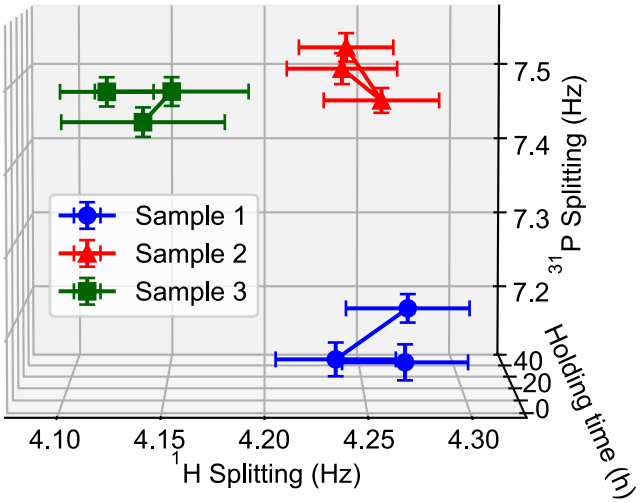

Fig. 14 Reproducibility and time-stability of diastereomeric splitting samples prepared in an identical manner. Three samples were prepared with identical ratios of FBTrp-S:FBTrp-R (80:20, 10 mM total concentration) and 10 mM P and measured using the same conditions as the samples used to construct the comagnetometer plot (figure **??**). From this it is clear that some variability of diastereomeric splitting is caused by sample preparation, possibly due to small differences in concentration. Fluctuations in Δ_d over the 48 h observation period are within the margin of error.

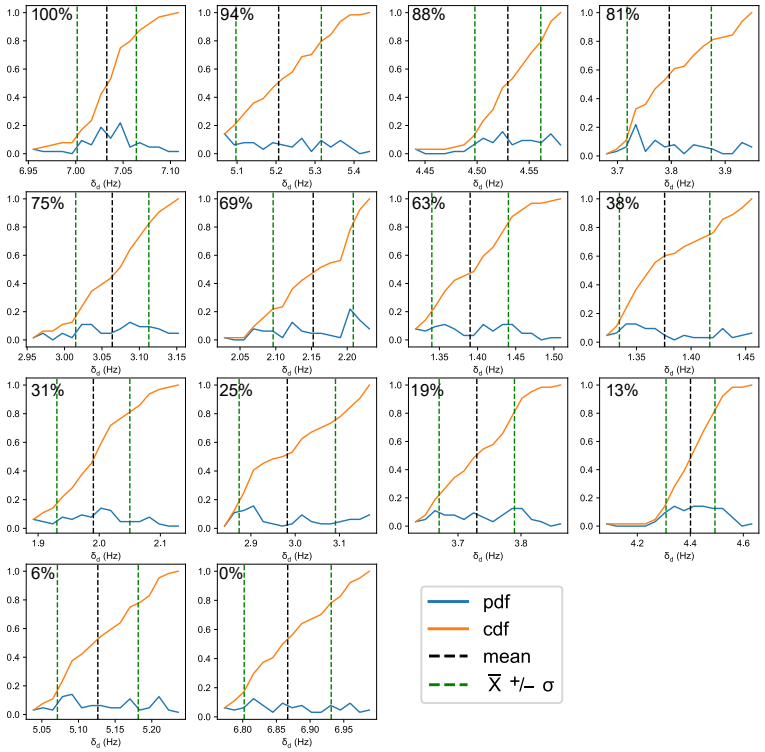

Fig. 15 Depiction of the probability distribution function (pdf, blue) and cumulative distribution function (cdf, orange) of diastereomeric splitting estimates from 64 ^{1}H spectra of each sample used to construct the second comagnetometer plot with bilinear rotation decoupling (BIRD). Deviations from a normal (Gaussian) distribution means that the data cannot be well described by basic statistical parameters like standard deviation, and could indicate the presence of systematic errors.

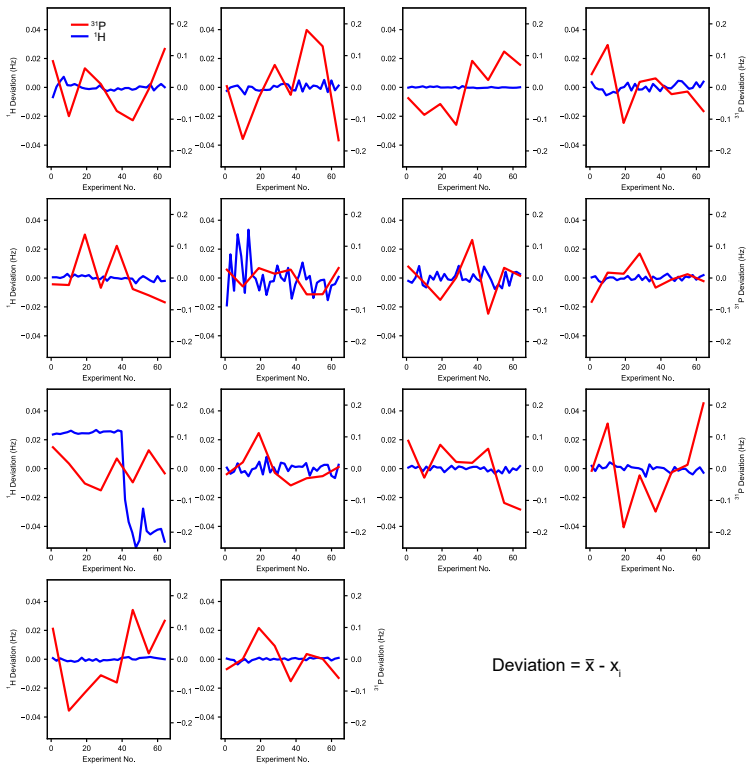

Fig. 16 Deviation of Δ_d from the mean extracted by fitting ^{1}H and ^{31}P (without ^{1}H decoupling) NMR spectra. ^{1}H and ^{31}P spectra were summed in groups of 2 and 8 respectively due to differences in signal-to-noise ratios which were lower for ^{31}P spectra. Clearly, there is larger variance in Δ_d extracted from ^{31}P spectra and it is likely that obtaining more spectra of less-sensitive nuclei (compared to ^{1}H) would help improve the confidence levels of fitting estimates. The systematic drift seen in ^{1}H Δ_d in the 3rd row, 1st column figure shows what may be a drift due to change in lineshape due to magnetic field homogeneity.

3 Fitting of proton and phosphorus NMR spectra

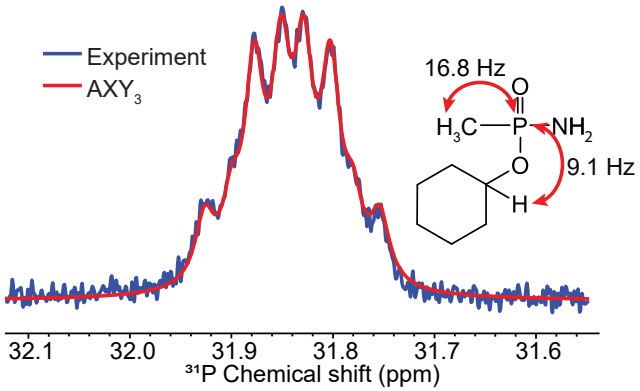

Fig. 17 Spectrum of chiral phosphorus probe with overlay of simulated line shape for an AXY_3 system. The trace in red is the result of fitting using ANATOLIA[1] which was used to estimate J-couplings and spectral line-widths for the spin system to generate a fitting function used to extract frequency estimates from non-^{1}H decoupled ^{31}P spectra.

For extraction of Δ_d ^{31}P and ^{1}H spectra were fit in python using the *curve_fit* package from *scipy.optimize*. For methyl-^{1}H peaks, a sum of complex Lorentzians with the general form

$$\sum_i^4 a_i \left(\frac{\Gamma^2}{\Gamma^2 + (\nu - \nu_{0i})^2} \cos(\phi_i) + \frac{\nu - \nu_{0i}}{\Gamma^2 + (\nu - \nu_{0i})^2} \sin(\phi_i) \right)$$

was used as the fitting function. Note that the amplitude (a), center frequency (ν_0), and phase (ϕ) are independent for each Lorentzian, while the width (Γ) is set to be the same for all peaks. This model generated the best fits judging by the residuals and by the variance estimates produced by the fitting algorithm. A sum of two Lorentzian doublets was also used but produced slightly larger error despite having fewer parameters compared to the four Lorentzian model.

The cyclohexyl peak was fit using a sum of two multiplets based on a J-coupling network of $^3J_{PH}$ = 9.13 Hz, $^3J_{HH}$ = 9.47 Hz, $^4J_{HH}$ = 4.002 Hz estimated from fitting with the two proton-proton J-couplings arising from methylene groups in the cyclohexyl moiety. The multiplets were generated using the Multiplet function of the nmrsim package in python[2].

Non-^{1}H-decoupled ^{31}P spectra were fit using a sum of two "doublets of quartets" assuming a 1:3:3:1 amplitude pattern typical of quartet peaks to reduce the number of parameters. The actual model used for fitting non-^{1}H-decoupled ^{31}P spectra is shown below.

```
def twoLorentzianMultiplet(v, center1, center2, FWHM, a1, a2, baseline, J_PH):
return (
(
  a1*(FWHM/(FWHM**2+(v-(center1-J_PH*3/2 - J_PNH/2))**2))
+ 3*a1*(FWHM/(FWHM**2+(v-(center1-J_PH/2 - J_PNH/2))**2))
+ 3*a1*(FWHM/(FWHM**2+(v-(center1+J_PH/2 - J_PNH/2))**2))
+ a1*(FWHM/(FWHM**2+(v-(center1+J_PH*3/2 - J_PNH/2))**2))
) +
(
  a1*(FWHM/(FWHM**2+(v-(center1-J_PH*3/2 + J_PNH/2))**2))
+ 3*a1*(FWHM/(FWHM**2+(v-(center1-J_PH/2 + J_PNH/2))**2))
+ 3*a1*(FWHM/(FWHM**2+(v-(center1+J_PH/2 + J_PNH/2))**2))
+ a1*(FWHM/(FWHM**2+(v-(center1+J_PH*3/2 + J_PNH/2))**2))
) +

(
  a2*(FWHM/(FWHM**2+(v-(center2-J_PH*3/2 - J_PNH/2))**2))
+ 3*a2*(FWHM/(FWHM**2+(v-(center2-J_PH/2 - J_PNH/2))**2))
+ 3*a2*(FWHM/(FWHM**2+(v-(center2+J_PH/2 - J_PNH/2))**2))
+ a2*(FWHM/(FWHM**2+(v-(center2+J_PH*3/2 - J_PNH/2))**2))
) +
(
  a2*(FWHM/(FWHM**2+(v-(center2-J_PH*3/2 + J_PNH/2))**2))
```

```
+ 3*a2*(FWHM/(FWHM**2+(v-(center2-J_PH/2 + J_PNH/2))**2))
+ 3*a2*(FWHM/(FWHM**2+(v-(center2+J_PH/2 + J_PNH/2))**2))
+ a2*(FWHM/(FWHM**2+(v-(center2+J_PH*3/2 + J_PNH/2))**2))
)

) + baseline
```

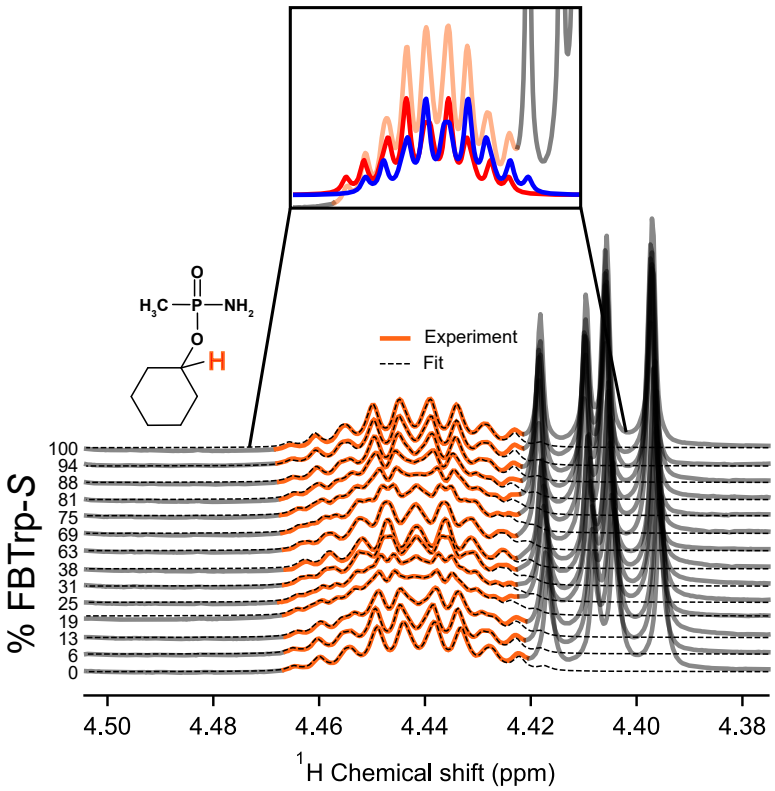

Fig. 18 ^{1}H spectra of the second multiplet from P which displays diastereomeric splitting. This multiplet originates from a single cyclohexyl proton nearest the ^{31}P center, highlighted in orange. Δ_d was extracted by fitting two analytical multiplet functions shown in the inset based on an assumed AM_2N_2X spin system.

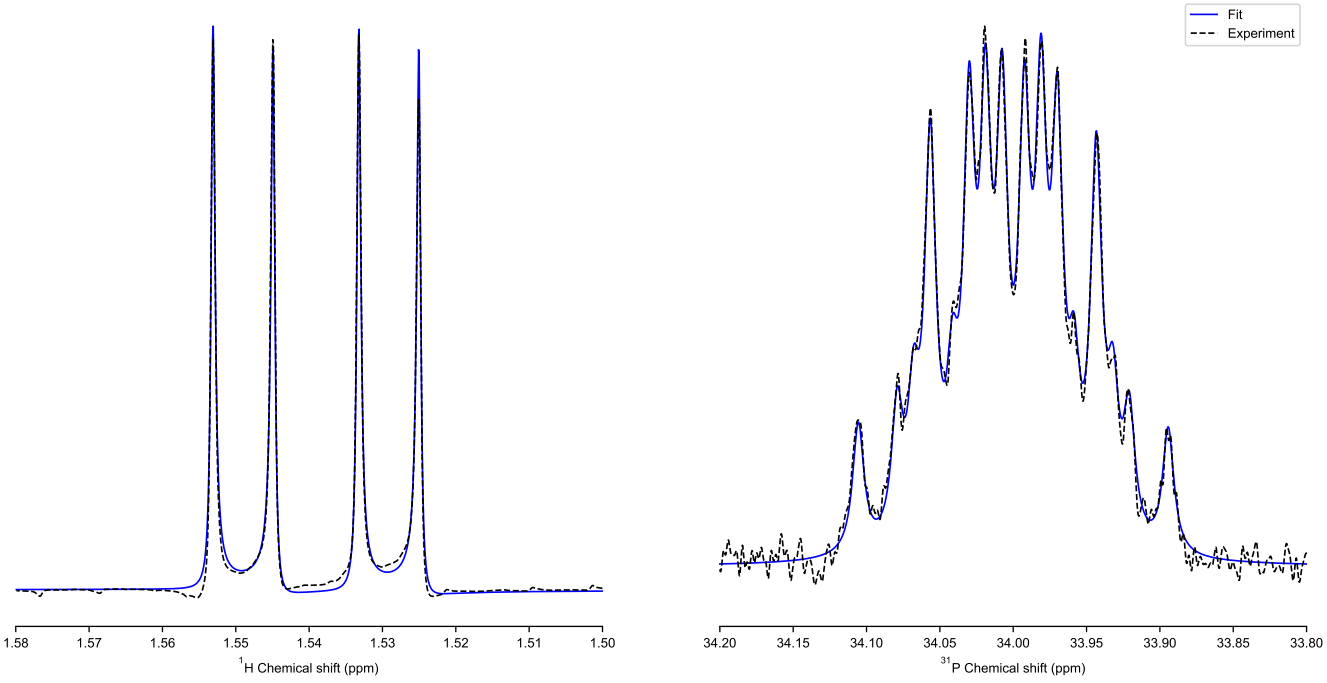

Fig. 19 Example plots of experimental data (10 mM P, 10 mM FBTrp-S in $CDCl_3$, 298 K, 20 T) fitted with Lorentzian functions to extract diastereomeric splitting.

4 BIRD pulse sequence

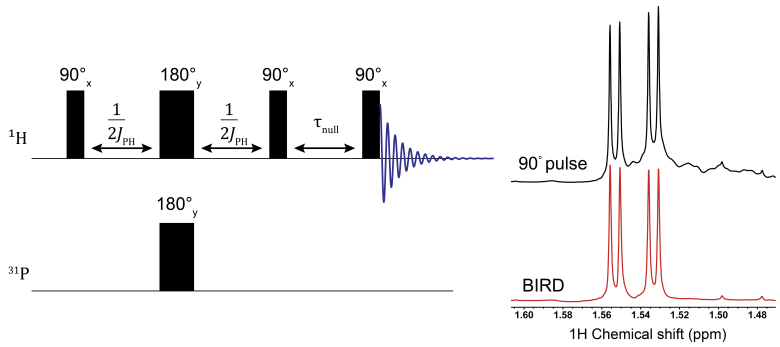

Fig. 20 Graphical depiction of the bilinear rotational decoupling (BIRD) pulse sequence used in proton spectral acquisition in the second titration. The object of the pulse sequence in this context is to orient all proton spins not coupled to ^{31}P opposite the applied magnetic field while leaving the spins coupled to ^{31}P along the applied field. A short delay before the final readout pulse is set to allow all spins aligned against the field to relax to zero, thus removing broad peaks overlapping the peaks of interest, allowing more precise modeling. Here, $^{2}J_{\mathrm{PH}}$ is the J-coupling between the methyl protons and phosphorus in the chiral probe molecule and τ_{null} is the waiting period to allow the z-component of spins not coupled to ^{31}P to relax until close to zero. Pulse sequences used $^{2}J_{\mathrm{PH}} = 16.7$ Hz and $\tau_{\mathrm{null}} = 100$ ms.

5 N,N-diethyl phosphorus probe molecule

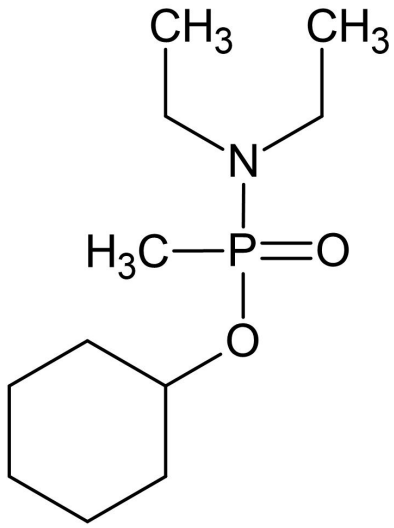

Fig. 21 Chemical structure of second chiral phosphorus compound examined in this study, cyclohexyl N,N-diethyl-*P*-methylphosphonamidate (DE-Phos). The ethyl groups substituted on the amino group are expected to reduce reactivity of the compound with respect to the protonated amino form. However, the conditions tested failed to produce diastereomeric splitting in ^{31}P spectra. Diastereomeric splitting was observed in ^{1}H spectra under several concentrations and ratios of DE-Phos and FBTrp.

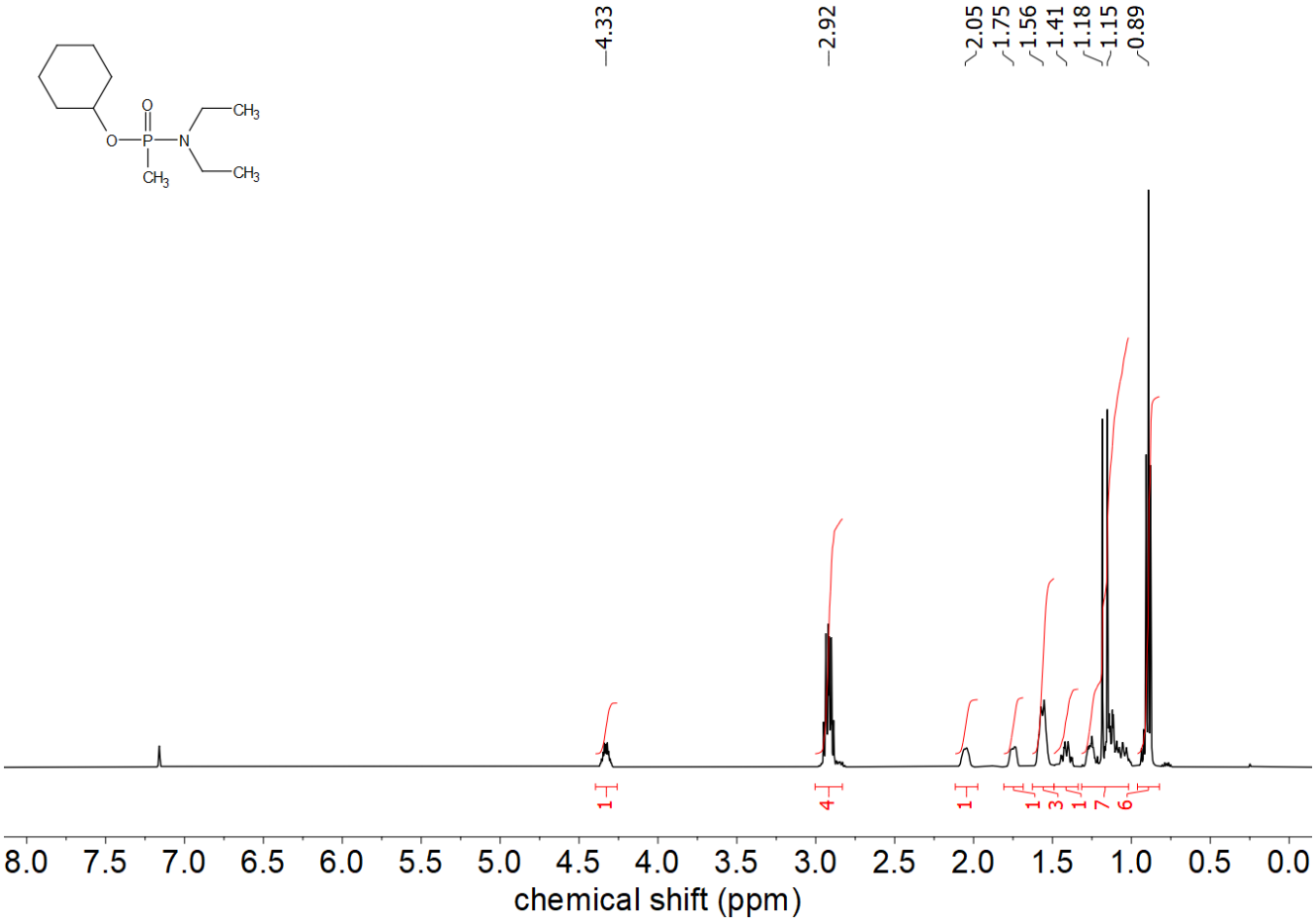

Fig. 22 ^{1}H NMR spectrum (500 MHz, C_6D_6) of Cyclohexyl *N,N*-diethyl-*P*-methylphosphonamidate.

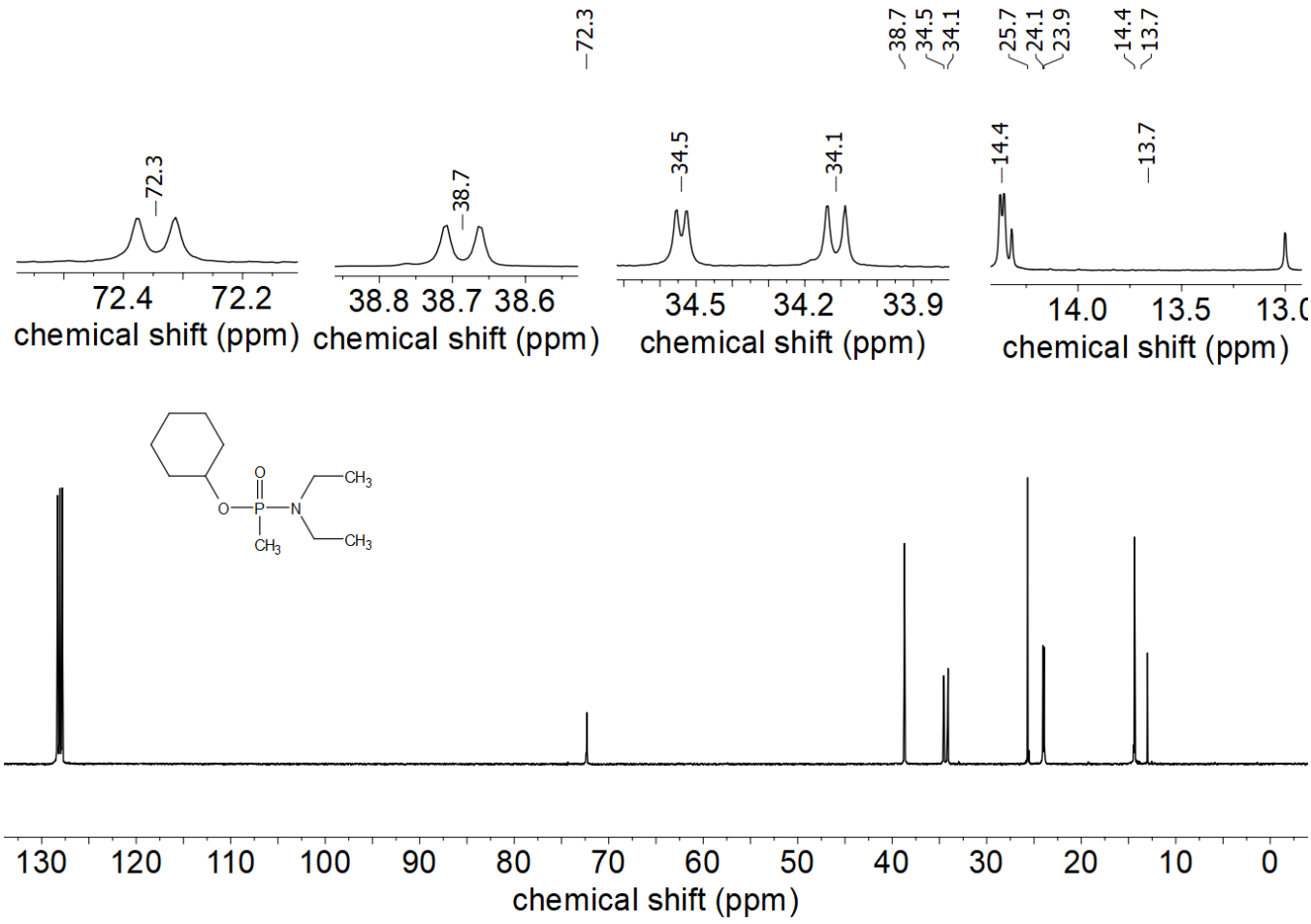

Fig. 23 ^{13}C NMR spectrum (101 MHz, C_6D_6) of Cyclohexyl *N*,*N*-diethyl-*P*-methylphosphonamidate with selected detail enlargement.

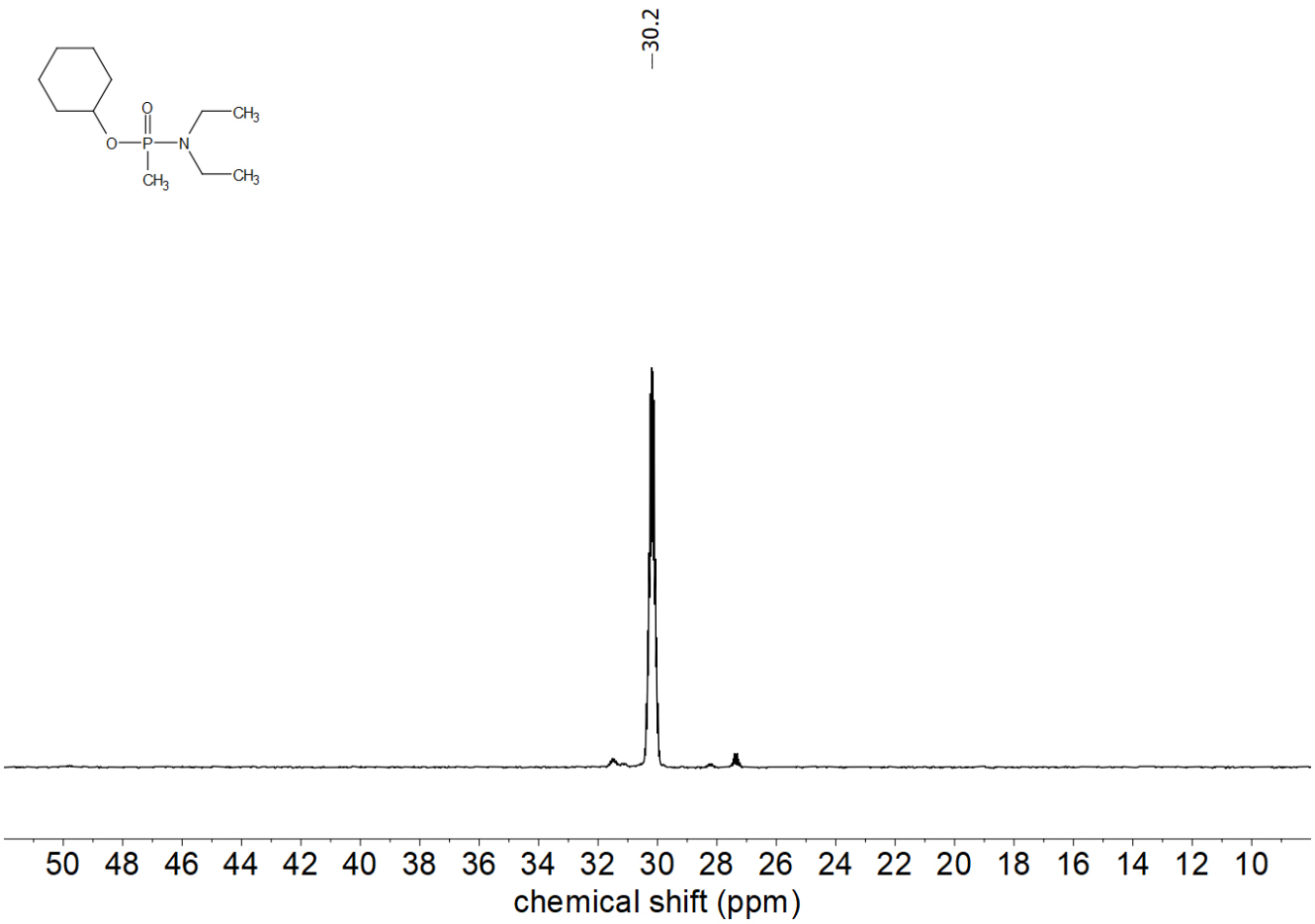

Fig. 24 ^{31}P NMR spectrum (202 MHz, C_6D_6) of Cyclohexyl *N*,*N*-diethyl-*P*-methylphosphonamidate.

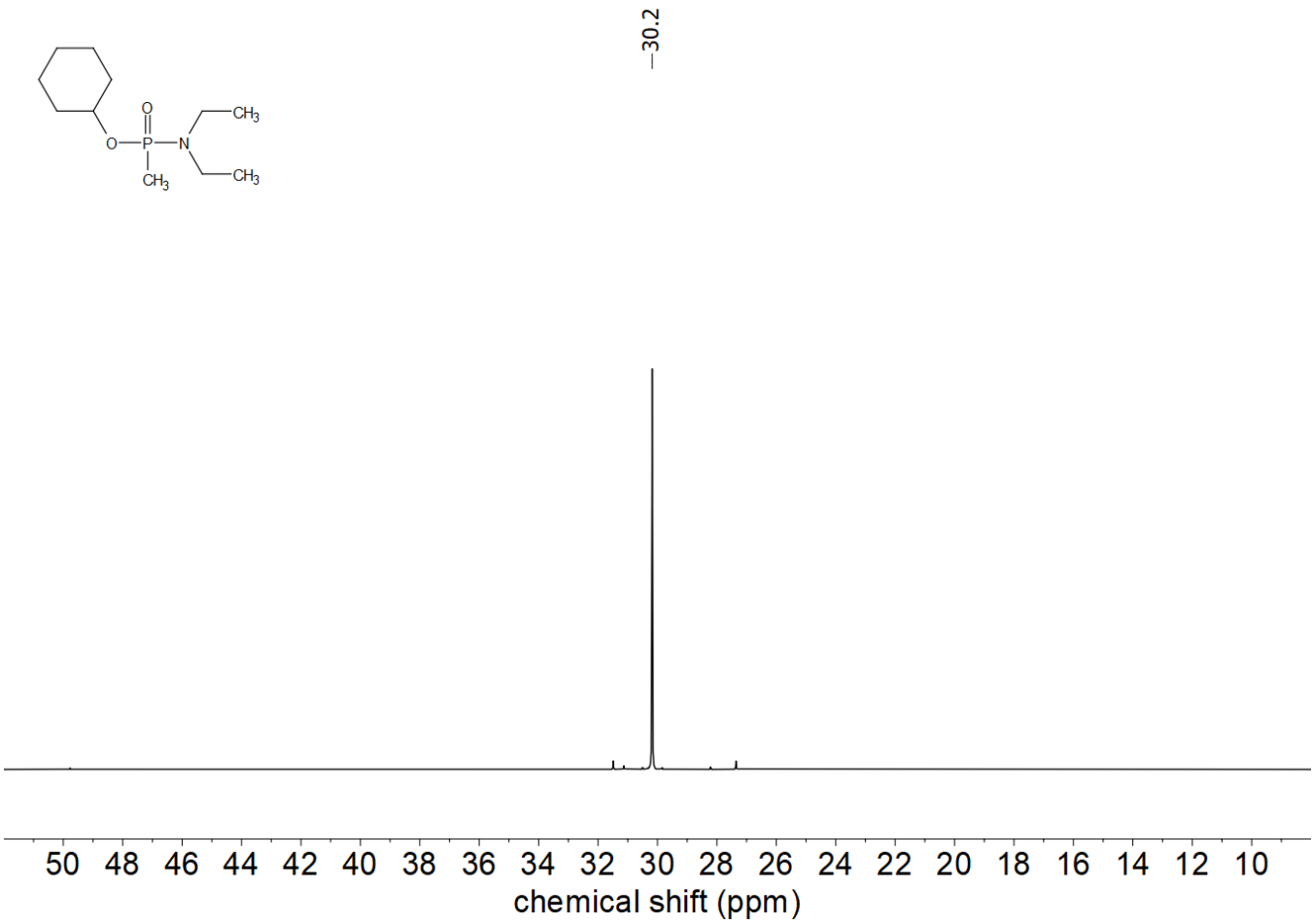

Fig. 25 $^{31}P\{^{1}H\}$ NMR spectrum (202 MHz, C_6D_6) of Cyclohexyl *N*,*N*-diethyl-*P*-methylphosphonamidate.

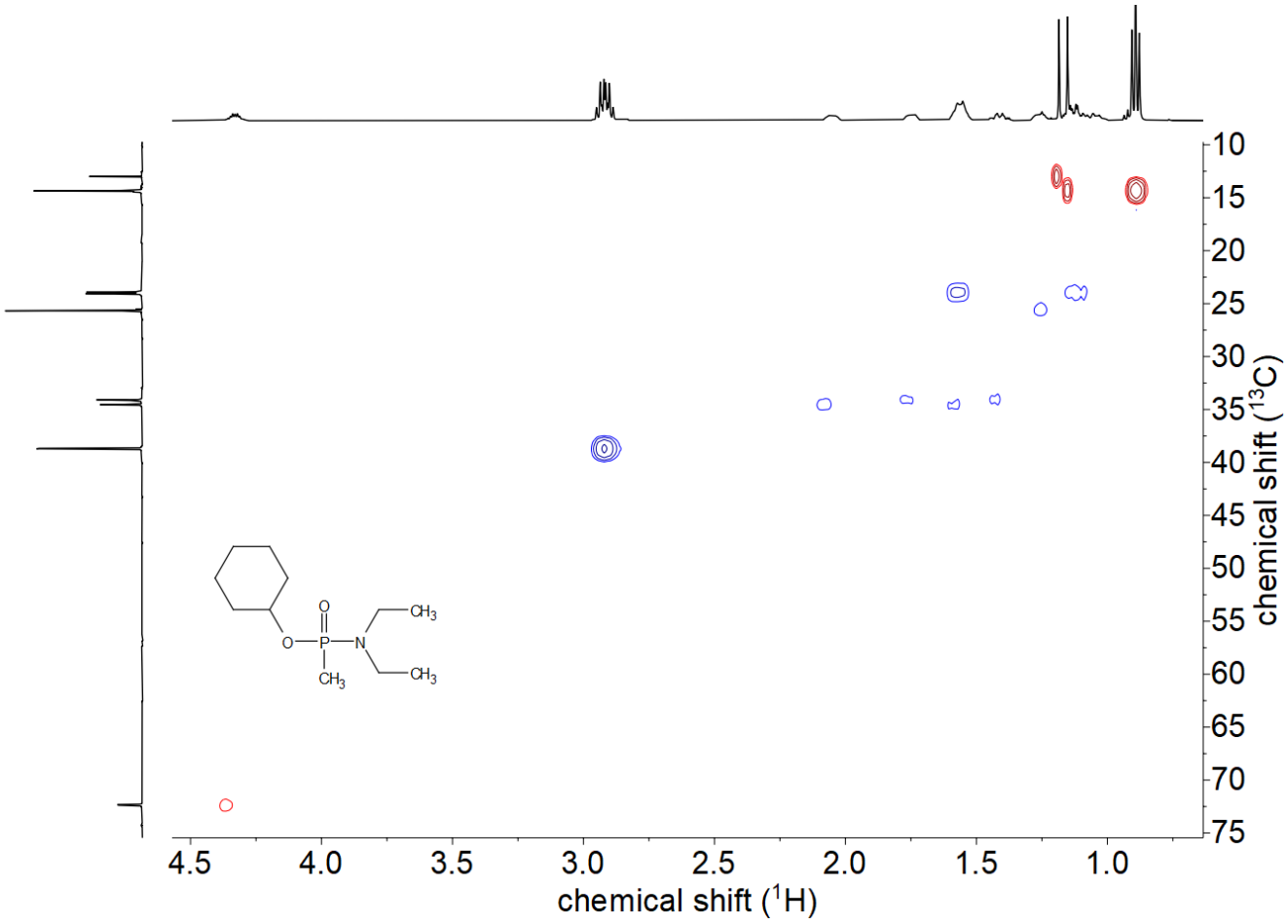

Fig. 26 2D-HSQC NMR spectrum (101 MHz, C_6D_6) of Cyclohexyl *N,N*-diethyl-*P*-methylphosphonamidate.

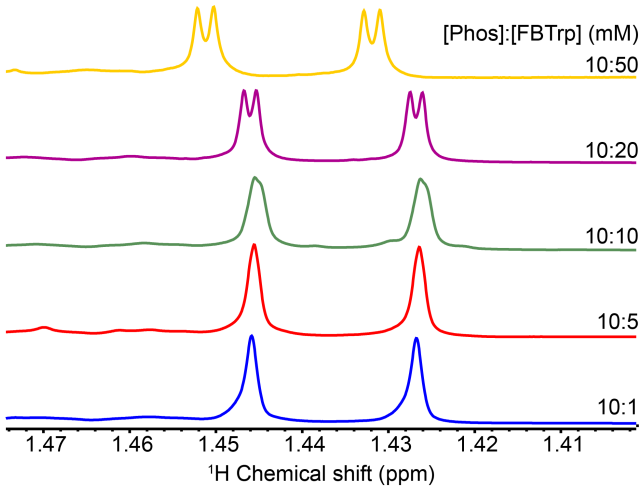

Fig. 27 Proton spectra at 20 T and 298 K of samples containing N,N-diethyl phosphorus chiral probe (DE-Phos) and FBTrp-S at several ratios. The concentration of DE-Phos was maintained constant at 10 mM while concentrations of FBTrp-S varied from 1 mM to 50 mM. Samples were prepared by mixing stock solutions of DE-Phos and FBTrp-S in chloroform directly in 5 mm NMR tubes and were allowed to equilibrate at room temperature for at least 1 hr.

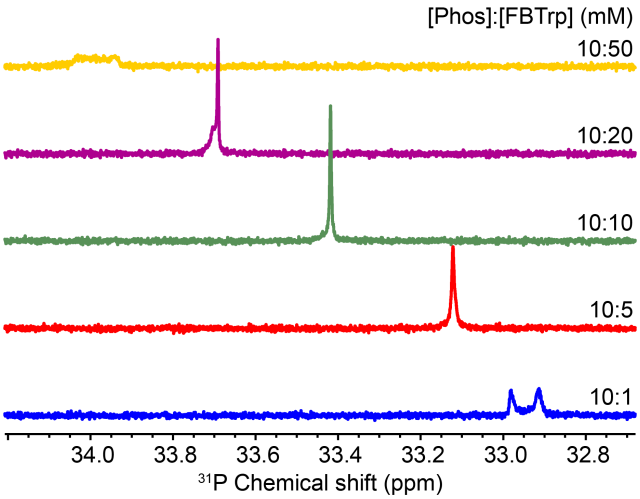

Fig. 28 ^{31}P spectra at 20 T and 298 K of samples containing ethylated phosphorus chiral probe (DE-Phos) and FBTrp-S at several ratios. The concentration of chiral probe was maintained constant at 10 mM while concentrations of FBTrp-S varied from 1 mM to 50 mM. Samples were prepared by mixing stock solutions of DE-Phos and FBTrp-S in chloroform directly in 5 mm NMR tubes and were allowed to equilibrate at room temperature for at least 1 hr.

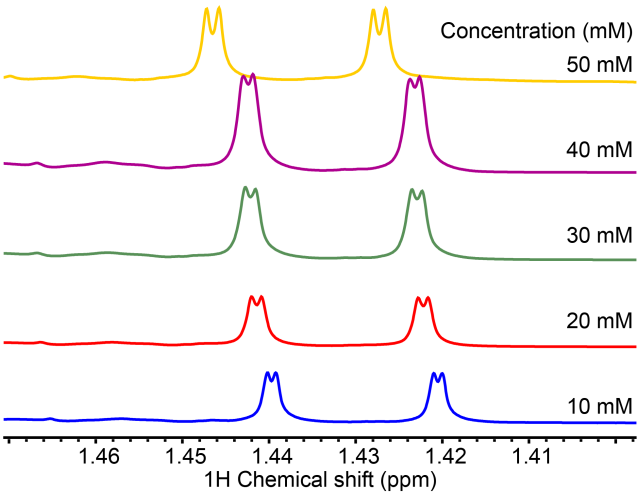

Fig. 29 ^{1}H NMR spectra showing the effect of increasing the concentration of FBTrp-S and DE-Phos in tandem at a 1:1 ratio in chloroform-d. A small increase in Δ_d is observed as the concentration is increased.

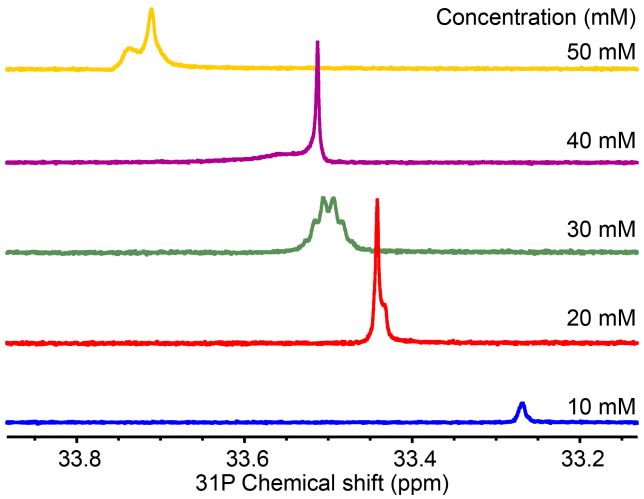

Fig. 30 ^{31}P NMR spectra showing the effect of increasing the concentration of FBTrp-S in tandem with DE-Phos at a 1:1 ratio in chloroform-d . Overall a shift towards higher frequency is observed, similar to that seen in P under the same conditions. None of the tested conditions were able to produce diastereomeric splitting in ^{31}P signals with DE-Phos.

Table 1 Relative energies ΔE_i with thermodynamic corrections of conformers of cyclohexyl *P*-methylphosphonamidate at the level of PBE0/def2-TZVPP and corresponding Boltzmann weights $w_i = \exp(-\Delta E_i/k_\mathrm{B}T)/[\sum_j \exp(-\Delta E_j/k_\mathrm{B}T)]$ at $T = 298.15$ K and 1 hPa pressure. NMR parameters computed at the level of 2c-ZORA-BHandH/[dyall.aae3z+sp(P,N,O,CH_3);IGLO-III] as described in the computational details section.

Conformer	ΔE/(kJ/mol)	w_i	$^1J_{^{31}\mathrm{P}-^{13}\mathrm{C}}$/Hz	$^2J_{^{31}\mathrm{P}-^1\mathrm{H}}$/Hz			$\delta_{^{31}\mathrm{P}}$/ppm	$\Delta_\mathrm{PV}\nu_{^{31}\mathrm{P}}$/μHz	$\Delta_\mathrm{PV}\nu_{^1\mathrm{H}}$/nHz		
1	0.2	0.324404	135.0	−14.0	−11.1	−12.3	25.7	−0.68	1.20	0.38	−0.75
2	0.8	0.257766	122.7	−9.8	−15.7	−9.7	22.2	−0.59	−0.52	0.89	0.49
3	1.9	0.166732	133.7	−13.2	−11.0	−12.0	25.1	−0.71	1.14	0.14	−0.60
4	2.2	0.146540	121.5	−9.9	−10.1	−14.9	21.4	−0.59	0.21	−0.45	0.89
5	3.5	0.087793	124.7	−10.0	−11.5	−12.5	28.0	−1.17	0.19	1.41	−1.84
6	9.1	0.009170	138.3	−15.0	−12.3	−11.3	26.9	−0.58	1.58	0.36	−1.19
7	10.3	0.005583	126.6	−9.0	−16.4	−10.9	22.1	−0.38	−0.93	1.01	0.77
8	14.1	0.001205	127.0	−10.4	−8.8	−16.3	19.1	−1.12	0.62	−0.17	1.08
9	16.5	0.000447	115.4	−9.0	−16.0	−8.3	22.4	0.56	−1.46	−1.21	2.31
10	18.0	0.000248	122.9	−12.0	−15.0	−7.9	18.8	−0.74	−3.00	0.63	2.78
11	24.0	0.000022	134.0	−10.9	−12.2	−13.7	25.3	−0.68	0.59	−0.81	1.11
12	25.3	0.000013	122.0	−10.1	−8.7	−15.2	20.9	−0.40	1.35	−1.52	1.32
13	25.3	0.000013	133.3	−12.0	−13.1	−10.9	24.2	−0.86	−0.18	0.90	0.04
14	25.4	0.000013	134.0	−12.3	−13.8	−10.9	25.3	−1.00	−0.67	1.06	0.12
15	25.6	0.000011	122.5	−15.2	−9.5	−10.0	21.8	−0.54	0.80	0.74	−0.67
16	25.6	0.000012	122.8	−15.6	−9.6	−9.7	22.0	−0.55	0.91	0.71	−0.61
17	26.0	0.000010	135.0	−12.4	−14.1	−11.2	25.5	−0.80	−0.78	1.14	0.33
18	26.3	0.000009	124.8	−16.1	−10.2	−10.3	21.9	−0.70	0.82	0.43	−0.48
19	26.9	0.000007	136.1	−14.4	−11.5	−12.5	25.5	−0.64	1.21	0.57	−0.79
20	33.7	0.000000	113.3	−16.9	−6.4	−9.1	18.0	0.25	−2.20	1.11	0.10
21	34.4	0.000000	127.7	−8.6	−16.5	−10.9	22.3	−0.23	−0.93	1.30	0.46
22	35.2	0.000000	113.0	−13.3	−7.6	−12.1	17.9	0.09	−2.15	1.97	1.16
23	36.3	0.000000	118.2	−12.0	−7.0	−15.0	15.9	−1.19	0.07	1.11	−0.41
Boltzmann weighted average			128.7	−11.8	−12.2	−12.0	24.2	−0.69	0.50	0.44	−0.25

Notes and references

1 D. Cheshkov, K. Sheberstov, D. Sinitsyn and V. Chertkov, *Magnetic Resonance in Chemistry*, 2018, **56**, 449–457.

2 G. M. Sametz, 2021.